

NON-RELATIVISTIC COLLISIONLESS SHOCKS IN UNMAGNETIZED ELECTRON-ION PLASMAS

TSUNEHICO N. KATO AND HIDEAKI TAKABE

Institute of Laser Engineering, Osaka University, 2-6 Yamada-oka, Suita, Osaka 565-0871, Japan
Draft version February 10, 2022

ABSTRACT

We show that the Weibel-mediated collisionless shocks are driven at non-relativistic propagation speed ($0.1c < V < 0.45c$) in unmagnetized electron-ion plasmas by performing two-dimensional particle-in-cell simulations. It is shown that the profiles of the number density and the mean velocity in the vicinity of the shock transition region, which are normalized by the respective upstream values, are almost independent of the upstream bulk velocity, i.e., the shock velocity. In particular, the width of the shock transition region is ~ 100 ion inertial length independent of the shock velocity. For these shocks the energy density of the magnetic field generated by the Weibel-type instability within the shock transition region reaches typically 1-2% of the upstream bulk kinetic energy density. This mechanism probably explains the robust formation of collisionless shocks, for example, driven by young supernova remnants, with no assumption of external magnetic field in the universe.

Subject headings: shock waves — plasmas — instabilities — magnetic fields

1. INTRODUCTION

Collisionless shocks are important phenomena in the universe; they heat and compress interstellar or intergalactic plasmas and often accelerate charged particles or cosmic rays. The dissipation mechanism of the collisionless shocks is highly complex and generally involved with instabilities in the collisionless plasma.

The Weibel instability is driven in anisotropic or counter-streaming collisionless plasmas (Weibel 1959; Fried 1959) and generates strong magnetic fields. Collisionless shocks inevitably generate an anisotropy within their transition region, where the upstream and downstream plasmas are mixed up, therefore, the Weibel instability can develop and generate strong magnetic fields there if the background magnetic field is weak. Moiseev & Sagdeev (1963) considered such a process in non-relativistic collisionless shocks and Medvedev & Loeb (1999) discussed the magnetic field generation by the Weibel instability in relativistic collisionless shocks of gamma-ray bursts.

In this context, the Weibel instability in relativistic counter-streaming plasmas has been investigated extensively by means of particle-in-cell simulations (e.g., Kazimura et al. 1998; Gruzinov 2001; Haruki & Sakai 2003; Silva et al. 2003; Nishikawa et al. 2003; Frederiksen et al. 2004; Spitkovsky 2005). Recent research with simulations showed that the “Weibel-mediated” collisionless shocks can form at relativistic propagation speed in electron-positron plasmas (Kato 2007; Chang et al. 2008) and also in electron-ion plasmas (Spitkovsky 2008) without background magnetic field; in these shocks the dissipation mechanism is effectively provided by the magnetic fields generated by the Weibel-type instability in the shock transition region. In the universe, these shocks can be driven associated with relativistic phenomena, such as gamma-ray bursts, jets from active galactic nuclei, or pulsar winds.

There is also a possibility that these Weibel-mediated shocks are driven even in non-relativistic phenomena,

e.g., shocks of supernova remnants whose propagation speed is typically $\sim 1,000 - 10,000$ km s⁻¹. However, in this case, the Weibel instability can be inefficient because the linear growth rate of the instability is proportional to the flow velocity V . Therefore, it is not clear yet whether this kind of shocks can exist in non-relativistic regime. In this paper, however, we show that the Weibel-mediated collisionless shocks propagating at non-relativistic speed can form in unmagnetized electron-ion plasmas by performing numerical simulations. This also suggests a possibility to proof the formation of these shocks in laboratory plasmas with large-scale laser facilities.

2. METHOD

In order to investigate the collisionless shocks in electron-ion plasmas without background magnetic fields, we performed numerical simulations. The simulation code is a relativistic and electromagnetic particle-in-cell code with two spatial and three velocity dimensions (2D3V) which was developed based on a standard method described by Birdsall & Langdon (1991). The basic equations are the Maxwell’s equations and the (relativistic) equation of motion of particles. The simulation plane is the $x-y$ plane. The z axis is perpendicular to the plane. Since we consider collisionless shocks in unmagnetized plasmas, the electromagnetic fields are initially set to zero over the entire simulation box. The boundary condition of the electromagnetic field is periodic to each direction.

In the simulations a collisionless shock is driven by means of the “injection method.” There are two rigid walls at the left-hand side (smaller x) and right-hand side (larger x) of the simulation box and these walls reflect particles specularly. Initially, both electrons and ions are uniformly loaded in the region between the two walls at the bulk flow velocity of V in the $+x$ -direction. At the early stage of the simulations, the particles located near the right wall were reflected by the wall and then interacted with the incoming particles, i.e., the upstream plasma, via some instabilities. Such instabilities induce strong electric or magnetic fields that provide dissipation

mechanism of the shock and, eventually, a collisionless shock is formed. Note that the frame of the simulation corresponds to the downstream rest frame.

3. RESULTS

We have carried out a series of simulations with upstream bulk velocities of $V = 0.45c$, $0.2c$, and $0.1c$, where c is the speed of light. The thermal velocity of electrons is typically taken as one-tenth of the bulk velocity and that of ions is determined so that the temperatures of electrons and ions are same. Because of the computational power, we used a reduced ion mass of $m_i = 20m_e$. Here, we take ω_{pe}^{-1} as the unit of time and the electron skin depth $\lambda_e \equiv c\omega_{pe}^{-1}$ as the unit of length, where $\omega_{pe} \equiv (4\pi n_{e0}e^2/m_e)^{1/2}$ is the electron plasma frequency defined for the electron number density of the upstream plasma, n_{e0} . We also define the ion inertial length, $\lambda_i \equiv (m_i/m_e)^{1/2}\lambda_e$. The units of electric and magnetic fields are both taken as $E_* = B_* \equiv c(4\pi n_{e0}m_e)^{1/2}$.

3.1. Results for $V = 0.45c$

The simulation for $V = 0.45c$ was performed on a grid of $N_x \times N_y = 4096 \times 512$ with ~ 27 particles per cell per species. The size of the simulation box is $L_x \times L_y = 2240\lambda_e \times 280\lambda_e$. (We choose the grid size so that the system is stable against the cold beam nonphysical instability, c.f. Birdsall & Langdon (1991).) The number density of ions obtained from the simulation at $\omega_{pe}t = 2100$ is shown in Fig. 1. The color shows the number density normalized by the upstream value, namely, n_{e0} . The upstream plasma flows from the left to the right and goes through the transition region which has a filamentary structure and then reaches the almost uniform downstream state ($x/\lambda_e > 1900$).

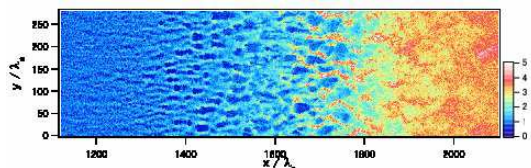


FIG. 1.— Number density of ions for the upstream bulk velocity of $V = 0.45c$ at $\omega_{pe}t = 2100$. The left-hand side and right-hand side are the upstream and downstream of the shock, respectively. Filamentary structure is visible in the shock transition region, $1300 < x/\lambda_e < 1900$.

Figure 2 shows the time evolution of the number density of ions. The number density shown in color is averaged over the y -direction. The transition region, or “shock front”, which is visible as a steep increase in the number density, propagates upstream at an almost constant speed ($\sim -0.18c$ measured in the downstream frame) after $\omega_{pe}t \sim 500$. Note that the particles that are reflected at the right wall at the early stage of the simulation, which are remains of the initial condition, eventually fade away at later times.

Figure 3 shows profiles of quantities averaged over the y -direction at $\omega_{pe}t = 2100$: (a) the ion number density, (b) the mean velocity in the x -direction, and (c) the energy densities of electric and magnetic fields. Both number density and mean velocity rapidly change to reach the downstream values through the transition region which

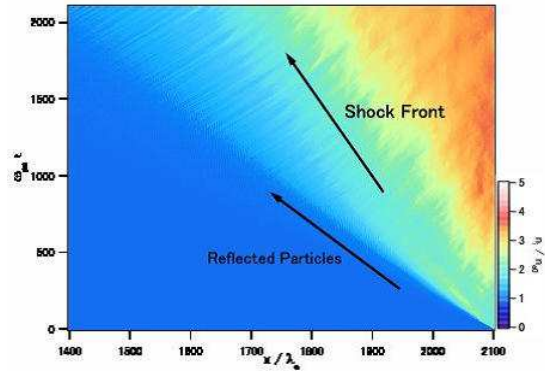


FIG. 2.— Time evolution of the number density of ions for $V = 0.45c$. The horizontal and vertical axes are the x -coordinate and the time, respectively. The color shows the number density averaged over the y -direction. The shock transition region, or “shock front”, is visible as a steep increase in the number density.

extends with the width of $W \sim 500\lambda_e$. It is remarkable that a strong magnetic field is generated within the shock transition region. The energy density of the magnetic field reaches approximately 1% of the upstream bulk kinetic energy density (measured in the downstream rest frame), $U_{KE} = n_{e0}(m_i + m_e)V^2/2$. This strong magnetic field deflects and isotropize the particles coming from upstream; this provides an effective dissipation mechanism for this collisionless shock.

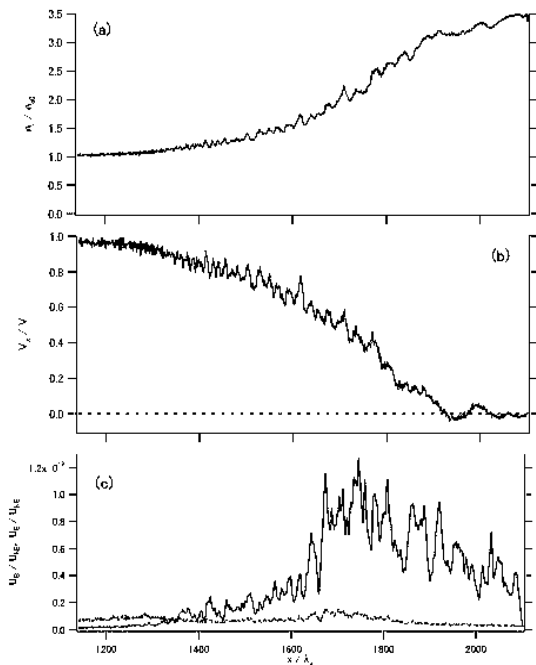


FIG. 3.— Profiles of (a) the ion number density, (b) the mean velocity in the x -direction both normalized by the respective upstream values, and (c) the energy densities of the magnetic (solid curve) and electric (dashed curve) fields both normalized by the particle bulk kinetic energy density of the upstream plasma.

Figure 4 shows the current density in the x -direction, J_x , and the z -component of the magnetic field, B_z , at $\omega_{pe}t = 2100$. It is evident that a number of current filaments exist within the transition region. These filaments consist of ions which are surrounded by the diffuse electrons similar to the case of the relativistic counter-

streaming plasmas (Frederiksen et al. 2004). The filamentary structure seen in the number density in Fig. 1 reflects the existence of them. As seen in the figure, these filaments generate the strong magnetic field around themselves which is also observed in Fig. 3 (c). This structure would be formed through the Weibel-type instability like the relativistic shocks in unmagnetized plasmas (Kato 2007; Spitkovsky 2008).

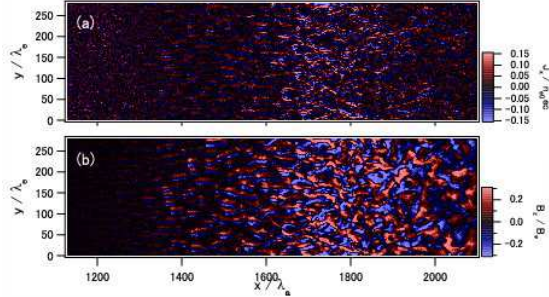


FIG. 4.— (a) The current density J_x and (b) the magnetic field B_z in the vicinity of the shock transition region at $\omega_{pe}t = 2100$.

3.2. Dependence on upstream bulk velocity and ion mass

We also performed simulations with the bulk velocities of $0.2c$ and $0.1c$. In both cases we confirmed that the structure of the shock is qualitatively identical to that of $V = 0.45c$ case. The ion number density and the magnetic field obtained for $V = 0.1c$ are shown in Fig. 5.

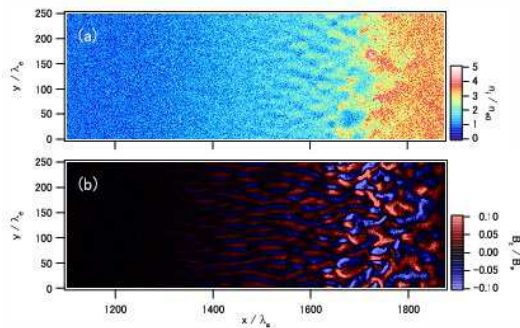


FIG. 5.— (a) The ion number density and (b) the magnetic field B_z obtained from the simulation for $V = 0.1c$.

It should be noted that these Weibel-mediated shocks have similarities in the profiles of some quantities under changing the upstream bulk velocity V . Figure 6 shows the profiles as Fig. 3 at different upstream bulk velocities: $V = 0.45c$, $0.2c$ and $0.1c$. Here, the horizontal axes are the x -coordinate normalized by the ion inertial length including the relativistic effect, $\lambda_i^* \equiv \Gamma^{1/2}\lambda_i$, where $\Gamma \equiv [1 - (V/c)^2]^{-1/2}$ is the Lorentz factor of the upstream bulk velocity. It is remarkable that the profiles in (a) and (b) are almost identical independent of V . In particular, the widths of the shock transition region are $W \sim 100\lambda_i^*$ in *all* cases. The energy densities of magnetic fields within the transition region also reach typically 1-2% of the upstream bulk kinetic energy density at maximum independent of V .

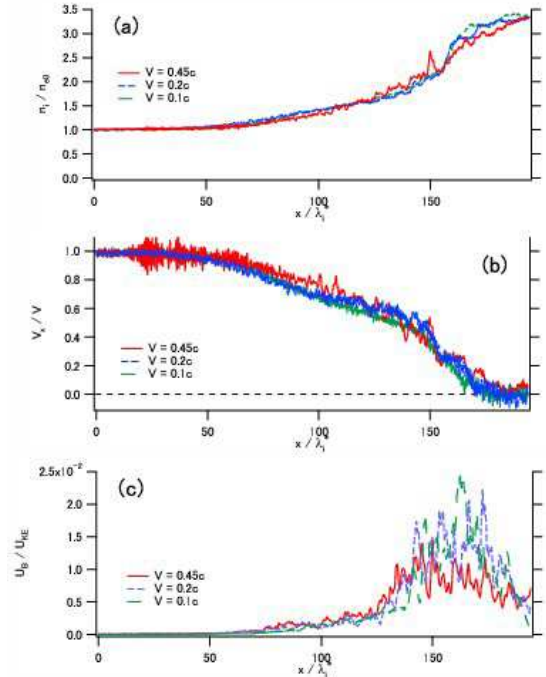


FIG. 6.— Profiles of (a) the ion number densities, (b) the mean velocities in the x -direction V_x , and (c) the energy densities of magnetic fields U_B for $V = 0.45c$ (red solid curves), $0.2c$ (blue short-dashed curves), and $0.1c$ (green long-dashed curves). The horizontal axes are the x -coordinate normalized by the ion inertial length (including the relativistic effect), λ_i^* . The normalizations of the profiles are same as in Fig. 3.

In order to see the effect of the mass ratio, we performed simulations for $m_i/m_e = 50$ and 100 with $V = 0.45c$. The normalized ion number densities for the different three mass ratios are shown in Fig. 7 as in Fig. 6 (a). The width of the transition region is approximately $W \sim 100\lambda_i^*$ in all cases and this suggests the width may be the same order even for the real mass ratio. However, there is a slight difference in the profiles and this will be investigated in detail in the forthcoming paper.

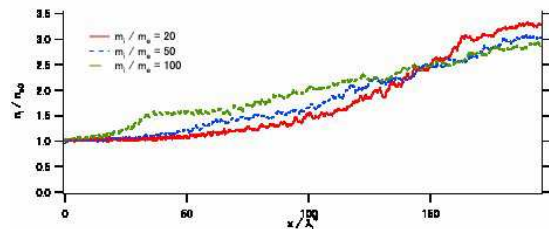


FIG. 7.— Profiles of the ion number densities for different ion-to-electron mass ratios: $m_i/m_e = 20$ (red solid curve), 50 (blue short-dashed curve), and 100 (green long-dashed curve). The upstream bulk velocities are $V = 0.45c$ in all cases. The horizontal and vertical axes are same as in Fig. 6 (a).

4. DISCUSSION

The similarities in the normalized profiles shown in Fig. 6 can be explained as follows. The structure of the transition region is essentially determined by the coalescence history of the ion current filaments. Here, we simply approximate the coalescence of two filaments as that of two straight currents. In this approximation, the

current in each filament is proportional to the bulk velocity V , and a dimensional analysis of the equation of motion of the filaments shows the time scale of the coalescence of two filaments due to the Lorentz force, τ , is proportional to V^{-1} . Thus, if we consider that the width in which the scale of the filamentary structure becomes twice is given by $\Delta W \sim V\tau$, it is independent of V . On the other hand, the downstream end of the transition region is determined by the saturation of the magnetic field of the ion current filaments; i.e., the typical gyro-radius of ions becomes comparable with the filament size, $r_{g,i} \sim r_f$, like the case of electron-positron current filaments (Kato 2005). This gives the condition $r_f \sim \lambda_i$, which is independent of V . Therefore, if we consider the initial scale of the ion current filaments is on the order of the electron skin depth λ_e , the total width of the transition region is also independent of V .

Though the results described in the previous section were obtained for unmagnetized plasmas, these Weibel-mediated shocks can also be driven in magnetized plasmas if the magnetic field is sufficiently weak. One of the criteria for neglecting the upstream background magnetic field, B_0 , may be given by $r_{g,i}/W \gg 1$, where $r_{g,i}$ is the typical gyro-radius of ions defined for B_0 and W is the typical width of the shock transition region. If we define the magnetization parameter σ as $\sigma \equiv [B_0^2/8\pi]/[n_{e0}(m_i + m_e)V^2/2]$ and use the result obtained in the previous section $W \sim 100\lambda_i^*$, the criterion can be rewritten $\sigma \ll 10^{-4}$. For shocks in su-

pernova remnants (SNRs) of ~ 1000 years old, typical parameters are $n_{e0} \sim 1 \text{ cm}^{-3}$, $V \sim 2000 \text{ km s}^{-1}$, and $B_0 \sim 3\mu\text{G}$. In this case, the magnetization parameter becomes $\sigma \sim 10^{-4} - 10^{-5}$ and therefore there is a possibility that the Weibel-mediated shocks are driven in SNRs. For younger SNRs with higher shock speeds of $\geq 10,000 \text{ km s}^{-1}$ (e.g., Reynolds et al. 2008), these shocks would be formed more easily.

If the Weibel-mediated shocks are driven even at the velocity of $\sim 1000 \text{ km s}^{-1}$, they can be investigated in laboratories because laser experiments are capable of generating collisionless plasma flow at this velocity (Nishimura et al. 1981; Ripin et al. 1990). For this plasma flow with $n_{e0} \sim 10^{20} \text{ cm}^{-3}$ (even at this density, the plasma can be collisionless during the shock formation), the width of the shock transition region is estimated to be $W \sim 2 \text{ mm}$. This is a reasonable value as the plasma size produced with the present-day large-scale laser facilities. To demonstrate the shock formation in laboratories is a challenging attempt but it would be particularly worthwhile as one of the key subjects for laboratory astrophysics (e.g., Takabe 2004).

We would like to thank Y. Sakawa and Y. Kuramitsu for their useful discussions and A. Kageyama for her helpful comments. Numerical computations were carried out at Cybermedia Center, Osaka University.

REFERENCES

- Birdsall, C. K., & Langdon, A. B. 1991, *Plasma Physics via Computer Simulation* (IOP Publishing: Bristol).
- Chang, P., Spitkovsky, A., & Arons, J. 2008, *ApJ*, 674, 378
- Frederiksen, J. T., Hededal, C. B., Haugbølle, T., & Nordlund, Å. 2004, *ApJ*, 608, L13
- Fried, B. D. 1959, *Phys. Fluids*, 2, 337
- Gruzinov, A. 2001, *ApJ*, submitted (astro-ph/0111321)
- Haruki, T., & Sakai, J. 2003, *Phys. Plasmas*, 10, 392
- Kato, T. N. 2005, *Phys. Plasmas*, 12, 080705
- Kato, T. N. 2007, *ApJ*, 668, 974
- Kazimura, Y., Sakai, J. I., Neubert, T., & Bulanov, S. V. 1998, *ApJ*, 498, L183
- Medvedev, M. V., & Loeb, A. 1999, *ApJ*, 526, 697
- Moiseev, S. S., & Sagdeev, R. Z. 1963, *J. Nucl. Energy C*, 5, 43
- Nishikawa, K.-I., Hardee, P., Richardson, G., Preece, R., Sol, H., & Fishman, G. J. 2003, *ApJ*, 595, 555
- Nishimura, H., et al. 1981, *Phys. Rev. A*, 23, 2011
- Reynolds, S. P., Borkowski, K. J., Green, D. A., Hwang, U., Harrus, I., Petre, R. 2008, *ApJ*, in press
- Ripin, B. H., et al. 1990, *Laser Part. Beams*, 8, 183
- Silva, L. O., Fonseca, R. A., Tonge, J. W., Dawson, J. M., Mori, W. B., & Medvedev, M. V. 2003 *ApJ*, 596, L121
- Spitkovsky, A. 2005, in *AIP Conf. Proc. 801, Astrophysical Sources of High Energy Particles and Radiation*, ed. T. Bulik, B. Rudak, & G. Madejski (New York: AIP), 345
- Spitkovsky, A. 2008, *ApJ*, 673, L39
- Takabe, H. 2004, *Nucl. Fusion*, 44, S149
- Weibel, E. S. 1959, *Phys. Rev. Lett.*, 2, 83